

Article

Source-to-Sink Comparative Study between Gas Reservoirs of the Ledong Submarine Channel and the Dongfang Submarine Fan in the Yinggehai Basin, South China Sea

Yue Yao ¹, Qiulei Guo ^{2,*} and Hua Wang ³

¹ College of Marine Science and Technology, China University of Geosciences, Wuhan 430074, China; missstaru@foxmail.com

² School of Earth and Space Sciences, Peking University, Beijing 100871, China

³ School of Earth Resources, China University of Geosciences, Wuhan 430074, China; wanghua@cug.edu.cn

* Correspondence: qiulei.guo@pku.edu.cn

Abstract: The Ledong submarine channel and the Dongfang submarine fan, two remarkable sedimentary systems developed during the late Miocene, are considered promising hydrocarbon reservoirs in the Yinggehai Basin of the South China Sea. A comparative study was conducted to reveal the differences between the source-to-sink characteristics of the two gas-bearing and gravity-driven depositional systems to determine their provenances, formation mechanisms and migration paths as well as their key controlling factors. The heavy mineral assemblages and detrital zircon U-Pb dating results suggest that the Ledong channel was fed by the Hainan provenance from the eastern margin, whereas the Dongfang fan was supplied by northwestern terrigenous sources. The relative sea level transgression and sufficient sediment supply triggered the delivery of deltaic loads toward the continental shelves. Seismic data show that fracture activity had a great impact on the tectono-morphologic features of the margins. During downward flow, the gravity flow along the Yingdong Slope encountered steeply falling faulted slope break belts and formed the Ledong incised channel, and the gravity flow of the Yingxi Slope moved through the gently dipping flexural break slope zone and formed the Dongfang dispersed lobe deposits. Since ca. 30 Ma, the sedimentary center has been migrating from the north to the southeast, which produced a clear control of the southeastward distribution pattern of these two sedimentary systems. Observations of cores and thin sections indicate that the rock structures and their compositions are more mature in the Dongfang channel than in the Ledong fan. This study documents significant differences and similarities by comparing the source-to-sink processes of the two gravity-driven systems that developed in the Yinggehai Basin and provides analogies for understanding similar submarine sedimentary systems that developed under similar geological contexts worldwide.

Keywords: submarine channel; submarine fan; source-to-sink; gas reservoirs; South China Sea; Yinggehai Basin



Citation: Yao, Y.; Guo, Q.; Wang, H. Source-to-Sink Comparative Study between Gas Reservoirs of the Ledong Submarine Channel and the Dongfang Submarine Fan in the Yinggehai Basin, South China Sea. *Energies* **2022**, *15*, 4298. <https://doi.org/10.3390/en15124298>

Academic Editor: Reza Rezaee

Received: 7 May 2022

Accepted: 7 June 2022

Published: 11 June 2022

Publisher's Note: MDPI stays neutral with regard to jurisdictional claims in published maps and institutional affiliations.



Copyright: © 2022 by the authors. Licensee MDPI, Basel, Switzerland. This article is an open access article distributed under the terms and conditions of the Creative Commons Attribution (CC BY) license (<https://creativecommons.org/licenses/by/4.0/>).

1. Introduction

Submarine fans and channels are prominent marine gravity flow sedimentary features; they compose the largest sediment accumulations on the continental margin and seafloor, which may be prolific hosts for oil and gas resources [1–5]. Worldwide, gravity flow systems were extensively developed during the Miocene icehouse periods, particularly in the basins of the South China Sea [6,7]. Some examples of Miocene submarine channels and fans are from the Pearl River mouth slope, the eastern Qiongdongnan margins, the Santos Basin and the south Greenland margin [1,2,8,9]. Both the Dongfang submarine fan and the newly discovered Ledong submarine channel, which developed in the late Miocene, are two important sweet spot zones in the Yinggehai Basin of the South China Sea, where numerous large gas fields have successively been discovered [10,11]. After years of

natural gas exploration, more than 260 billion cubic meters of proven natural gas reserves have been confirmed in the Dongfang and Ledong districts [12,13]. Similar to many terrestrial, lacustrine and marine basins around the world, the Yinggehai Basin is a multisource supply basin with diverse surrounding river systems and complex lithologic distributions [14–16]. The two sedimentary systems present very different characteristics with respect to morphology, provenance, transport pathways and sedimentary characteristics. Therefore, it is of great significance and a great necessity to conduct a comparative study of the “source-route-sink” processes of these two typical gravity flow sedimentary systems.

The concept of source-to-sink links together all of the steps from sediment formation to final deposition, with regard to the denudation of sources, the transfer of erosion products and the ultimate sedimentation process [17–20]. Previous researchers have discussed the source-to-sink system of the Yinggehai Basin and have confirmed two major sources of the basin, one being the Yangtze and Indosinian plates in the northwestern part of the basin and the other being the Hainan Island uplift in the eastern part of the basin [21–24]. However, little attention has been given to the similarities, differences and correlations of the source-to-sink processes among different submarine sedimentary systems. Specifically, no systematic source-to-sink comparative study on the Ledong gravity flow channel system and Dongfang submarine fan system has been conducted. Hence, it is necessary to strengthen the comparison and summarize the regularity of sediments under different source and sink modes. Scholars have conducted detailed studies of the sedimentary system developed in the Ledong and Dongfang districts [25–27]. For example, Huang et al. (2021) [25] studied the depositional facies, logging facies and petrographic characteristics of the submarine fan developed in the Dongfang district. Li et al. (2021) [12] studied the filling evolution characteristics of axial gravity flow channels in the Ledong district. Nonetheless, the controlling agents for the differences in the sedimentary systems in the submarine fans, which dominate the Dongfang area, and the gravity flow channels, which dominate the Ledong area, are still under a dense fog. More work is needed to explain the differences in the material sources and migration processes of the sediments between the two and to reveal the dissimilarities in their formation mechanisms.

This study aims to systematically compare and clarify the differences and develop correlations between the “source–sink” processes of these two typical gas-bearing and gravity-driven sedimentary systems that developed in the Miocene Huangliu Formation in the Ledong and Dongfang districts of the Yinggehai Basin with macroscopic to microscopic petrological analyses, heavy mineral assemblages, zircon U-Pb dating, combined well logging and seismic analyses. Specifically, from the source–sink perspective, the potential origin, triggering mechanism, transport path and depositional characteristics have been investigated. The study discusses why two different types of submarine gravity flow systems developed in the same basin during the same geological time and whether there was a key controlling factor influencing the development and distribution patterns of the channels and lobes. This study aims to develop some valuable geological guidance for future explorations for gas reservoirs in the South China Sea and to be an important reference to allow investigators to predict the evolution of other comparable sedimentary systems in analogous depositional environments.

2. Geological Setting

2.1. The Yinggehai Basin

The Yinggehai Basin (Figure 1a) in the South China Sea is an important Cenozoic hydrocarbon-bearing basin located on the northwestern margin of the South China Sea between Hainan Island and the Indo-China Peninsula [28–30]. Unlike the Beibuwan, Qiongdongnan and Zhujiangkou basins in the western part of the South China Sea, the Yinggehai Basin has a unique NNW–SSE trend, with an area of $12.17 \times 10^4 \text{ km}^2$ [31–33]. The Yinggehai Basin is a transformation extensional basin formed in the early Eocene by the superposition of various tectonic movements, such as the subduction of the Indian plate into the Eurasian plate, the uplift of the Qinghai-Tibet orogen and the expansion

of the South China seafloor [24,30]. The basin features a high geothermal gradient (4 to 6 °C/100 m), a large-scale anomalous pressure coefficient (1.0 to 2.3), rapid subsidence (500 to 1400 m/Ma) and mud diapering [34,35].

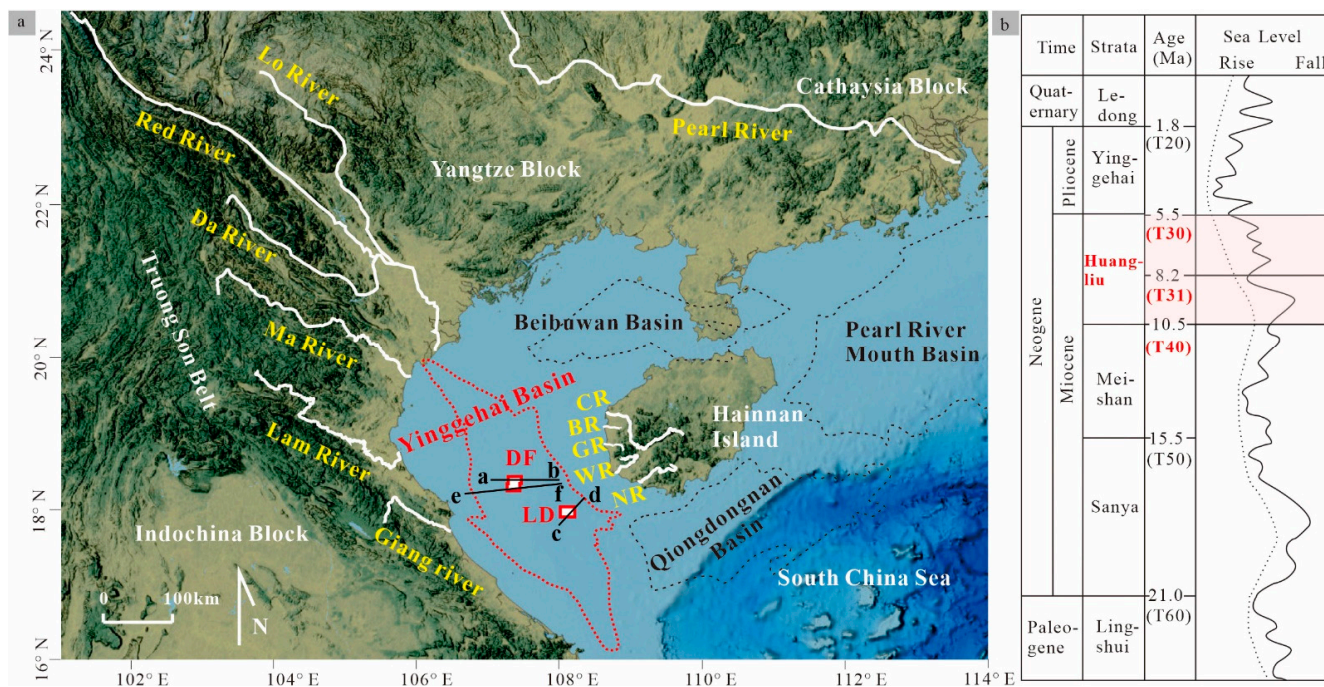


Figure 1. (a) Topographic map showing the location of the Yinggehai Basin, which is in the north-western part of the South China Sea, and the adjacent continental blocks, sedimentary basins and major drainage systems. DF: Dongfang, LD: Ledong, NR: Ningyuan River, WR: Wanglou River, GR: Ganen River, BR: Beili River, CR: Changhua River. (a–b, c–d, e–f are seismic lines). (b) Stratigraphic chart with sea-level curve (modified from Huang et al. (2020) [11]). T20, T30, T40, T50 and T60 represent the seismic boundaries between the different formations, and the studied strata of the Huangliu Formation are highlighted in the chart. T30 and T40 are the top and bottom surface layers of the Huangliu Formation, respectively, whereas T31 divides the Huangliu Formation into the upper member and lower member.

At present, a relatively complete Cenozoic stratum has been established in the Yinggehai Basin. The stratigraphy from Paleogene to Quaternary are the Lingshui, Sanya, Meishan, Huangliu, Yinggehai and Ledong Formations (Figure 1b) [36,37]. Among these, the late Miocene Huangliu Formation (10.5–5.5 Ma) is located between the basin-wide unconformities, namely, the T40 and T30 seismic boundaries, which are further divided into upper and lower segments by the T31 surface, dated at 8.2 Ma (Figure 1b).

The Yinggehai Basin is divided into three tectonic units (Figure 2), which are the Yingxi Slope, the Central Depression and the Yingdong Slope, by the Yingxi Fault zone in the west and the No. 1 Fault zone in the east [28,30]. The Yingxi Fault zone is subdivided into the Da, Ma, Lam, Truong Son faults, etc. The No. 1 Fault zone is subdivided into the Yingdong Fault and the No. 1 Fault (Figure 2) [38,39]. The fault system in the basin is complex, and the trends of these fault zones are mainly SSE–SE, among which the No. 1 Fault zone on the east side of the basin is dominant in the basin and is a large basin-controlling fault that developed in a SE trend.

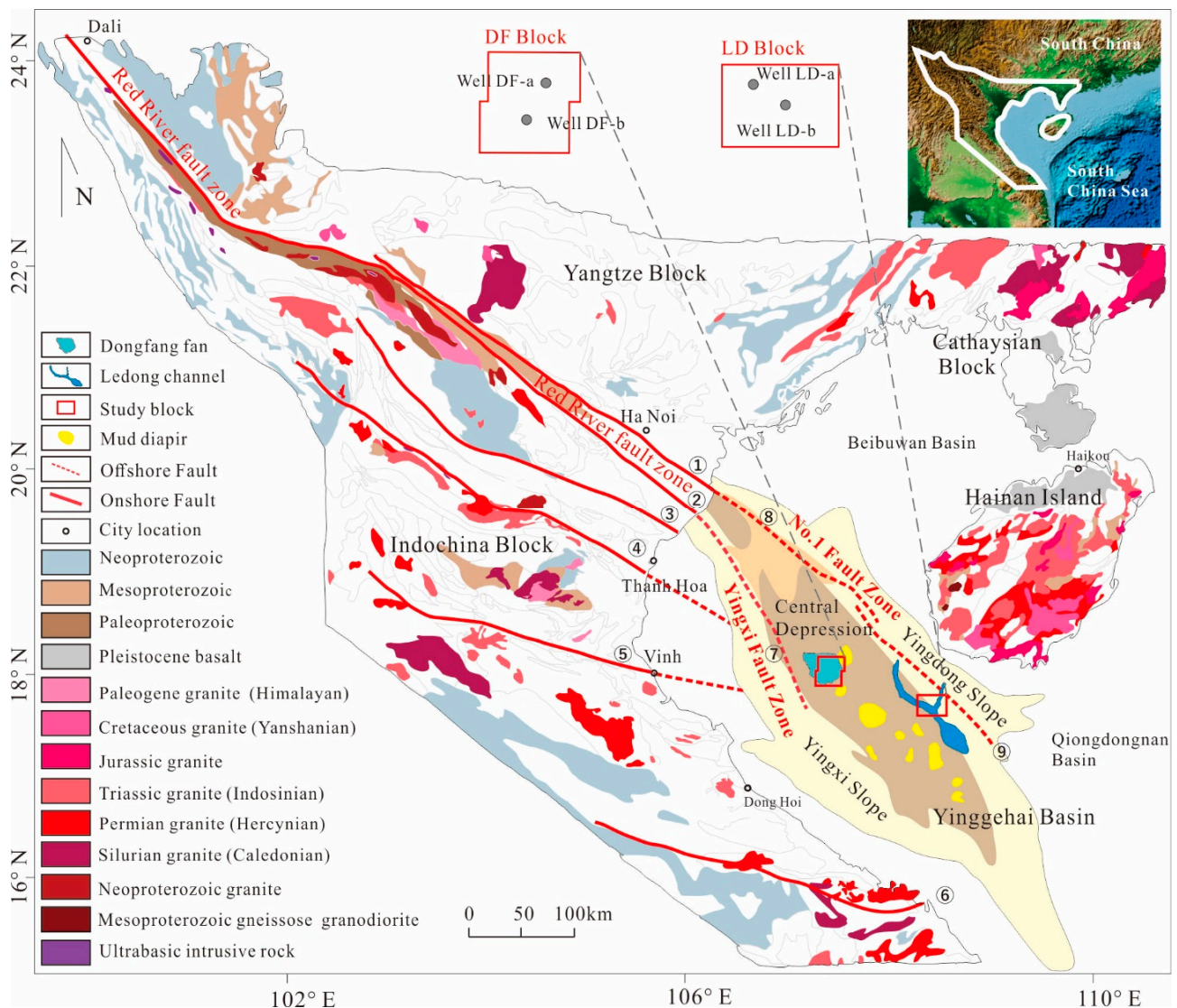


Figure 2. Igneous and Proterozoic rocks are distributed around the Yinggehai Basin. The Dongfang Block and submarine fan of this study are located in the Central Depression, and the Ledong Block and submarine channel are located beside the Yingdong Slope. Some major onshore faults are shown, which include the ① Lo River Fault, ② Red River Fault, ③ Da River Fault, ④ Ma River Fault, ⑤ Lam River Fault, ⑥ Truong Son Fault, ⑦ Yingxi Fault, ⑧ Yingdong Fault and ⑨ No. 1 Fault. The No. 1 Fault zone comprises the Yingfong Fault and the No. 1 Fault. The small map in the upper right corner shows the regional location of the geological map.

The Yinggehai Basin had sufficient material sources from the numerous nearby river systems (Figure 1a). The provenance mainly consists of the Red River source from the Yangtze Plate in the northern part of the Yinggehai Basin, the Truong Son Belt source along the coast of Vietnam in the west and the Hainan source from Hainan Island in the east (Figure 1a) [40–42]. The Truong Son Belt and the Red River source are collectively referred to as the northwestern provenance. The current northwestern provenance river system is relatively large, among which the Red River drainage includes the Red River, Da River and Lo River, and the Truong Son Belt drainage includes the Ma River, Lam River and Giang River (Figure 1a). There are many river systems along the west coast of Hainan Island, including the Changhua River, Beili River, Ganen River, Ningyuan River and Wanglou River.

The Truong Son Belt developed in the eastern margin of Vietnam and spreads in an “S” pattern from north to south. Due to high gravitational potential energy, the sand contents of Vietnam rivers are generally high [43,44]. The northern part of the basin is dominated by Red River source input. Moreover, after its upper reaches were captured by the Yangtze River (before the early Miocene), the Miocene source area shrunk somewhat from its previous extent, but its source supply capacity was still large [7]. The Hainan Island Uplift was formed in the early Cretaceous period and is mainly located in the central and southern parts of Hainan Island, with east–west fault zones on both sides, covering an area of $3.44 \times 10^4 \text{ km}^2$, and the current height of Wuzhishan, its main peak, is approximately 1887 m [45,46].

2.2. The Dongfang Submarine Fan and Ledong Submarine Channel

Exploration practice has shown that the Huangliu Formation in the Yinggehai Basin is the most developed section of gravity flow [10,25]. The sea level dropped (Figure 1b) during this period, and the coastline migrated toward the basin, which was conducive to the long-distance transport of clastic material to be deposited in the depression.

The Dongfang Block (Figure 2) is located in the north-central part of the Central Depression of the Yinggehai Basin, near the central mud diapir anticline structure, with a total area of approximately 2400 km^2 [6,23]. Multiple submarine gravity flow fan sedimentary systems developed in the Huangliu Formation of the Dongfang district, and the submarine fan of this study is located in the Dongfang Block (Figure 2). The submarine fan covers an area of approximately 700 km^2 and is distributed in a NW–SE orientation. It developed in the first member of the upper Miocene Huangliu Formation between seismic interfaces T30 and T31 (Figure 1b).

The Ledong Block (Figure 2) is located between the Yingdong Slope belt and the Central Depression belt of the Yinggehai Basin in the western continental shelf of the northern part of the South China Sea [26,47]. This block is currently in the exploration evaluation stage, and the main gas-bearing zone is the Huangliu Formation. The submarine gravity flow channel is located in the second member of the Upper Miocene Huangliu Formation, which is located between the seismic interface T31–T40 (Figure 1b), with a depth of 3800–4500 m, which was deposited in a shallow sea sedimentary environment. The channel consists of two branches: the north branch and the east branch (Figure 2). The east branch developed parallel to the Yingdong slope, and the north branch is perpendicular to the slope. Overall, the channel is approximately 190 km in length, 2–7.2 km in width and 80–550 m in depth. The northern and southern branches intersect on the slope and continue to develop axially toward the southeast for nearly 20 km before they begin to disperse, with the tail disappearing in a fan-like pattern in the combination zone of the Yinggehai and Qiongdongnan basins.

3. Data and Method

There is currently a total of 23 wells drilled in the Ledong and Dongfang study areas. However, due to the difficulty and limitations of coring in offshore engineering projects, there are currently only four coring wells in the study area. Through this study, the well logging curves, cores, rock cuttings and rock slice samples from the four most typical wells in the Dongfang and Ledong districts were selected for comparative analysis, including Well DF-a and Well DF-b drilled in the Dongfang submarine fan and Well LD-a and Well LD-b drilled in the Ledong submarine channel (Figure 2).

During the field investigations, five river estuary sand samples were collected on the west side of Hainan Island from the Ningyuan River, Wanglou River, Beili River, Ganen River and Changhua River (Figure 1). Data from the Red River and eastern Vietnam River groups riverbank sand samples were gathered from Fyhn’s published reports [44]. Eight core samples were selected for heavy mineral composition analysis, and four samples among them were selected for zircon U–Pb dating analysis. Details about the data for zircon dating and heavy mineral analyses are listed in Table 1. The seismic data for the Ledong

and Dongfang districts were provided by the China National Offshore Oil Corporation (Hainan Branch). The poststack 3D seismic data, having a bin size of $12.5 \times 12.5 \text{ m}^2$ and a full fold value of 48, used in this study were acquired between 2001 and 2015. Datasets were characterized by an effective frequency range of 15–55 Hz, with a predominant frequency of approximately 40 Hz.

Table 1. Zircon and heavy mineral sample details.

Sample	Name	Origination	Depth	Location	Formation
Dongfang Sample	DF-a	Borehole rock cuttings	2876 m	Dongfang fan	Huangliu T31-T30
	DF-a-2	Borehole rock cuttings	2832 m	Dongfang fan	Huangliu T31-T30
	DF-b	Borehole rock cuttings	3120 m	Dongfang fan	Huangliu T31-T30
	DF-b-2	Borehole rock cuttings	3156 m	Dongfang fan	Huangliu T31-T30
Ledong Sample	LD-a	Borehole rock cuttings	4104 m	Ledong channel	Huangliu T40-T31
	LD-a-2	Borehole rock cuttings	4180 m	Ledong channel	Huangliu T40-T31
	LD-b	Borehole rock cuttings	4072 m	Ledong channel	Huangliu T40-T31
	LD-b-2	Borehole rock cuttings	4158 m	Ledong channel	Huangliu T40-T31
Hainan Island Sample	NR	Ngyuan River sand	Surface	Hainan estuary	Quaternary
	WR	Wanglou River sand	Surface	Hainan estuary	Quaternary
	CR	Changhua River sand	Surface	Hainan estuary	Quaternary
	BR	Beili River sand	Surface	Hainan estuary	Quaternary
	GR	Ganen River sand	Surface	Hainan estuary	Quaternary
Northwest Provenance Sample	Red	Red River sand	Surface	Riverbank	Quaternary
	Ma	Ma River sand	Surface	Riverbank	Quaternary
	Lam	Lam River sand	Surface	Riverbank	Quaternary
	Giang	Giang River sand	Surface	Riverbank	Quaternary

The detrital zircon U/Pb dating method, heavy mineral assemblage method, core and sandstone thin section observations and other regional geological data were combined to determine the rock compositions and potential detrital material source areas. Samples were sent to the Langfang Geological Service Co., Ltd., Langfang, China, for zircon and heavy mineral identification, separation and counting. In this study, ten types of heavy minerals with relatively high and comparable contents were screened from the samples, including extremely stable heavy minerals such as zircon, tourmaline and rutile; stable heavy minerals such as garnet, sphene, magnetite, leucoxene, anatase, monazite and staurolite; and unstable minerals such as chlorite and pyroxene [41,48]. The study calculated the relative weight percentages of the heavy minerals as well as the zircon–tourmaline–rutile (ZTR) index, which measures the maturity of heavy minerals [49]. Heavy minerals with great maturity (such as zircon, rutile or tourmaline) have strong resistance to weathering and can, essentially, maintain their original properties after long-distance transportation and screen-

ing [21]. In situ zircon U-Pb isotope dating was carried out at Wuhan Shangpu Analytical Technology Co., Ltd., Wuhan, China, by using an Agilent 700 Inductively Coupled Plasma Mass Spectrometer and a GeoLas HD coherent 193 nm excimer laser ablation system. The test used international standard material samples 91,500, GJ-1 and NIST610 as the isotope ratio calibration standard sample, the isotope ratio monitoring standard sample and the trace element calibration standard sample, respectively. The processing software used was ICPMSDATA CAL10.8. U-Pb ages with concordance values greater than or equal to 90% were retained for zircon dating in the study.

Through the seismic preprocessing and interpretation method, the internal structure of the sedimentary system and the basin's tectono-morphologic characteristics were analyzed. Schlumberger's Geoframe software was applied to visualize the subsurface structure through a three-dimensional seismic reflection structure, amplitude strength and stratigraphic continuity profile. The faulting system, morphology of the continental shelf and gravity flow in the Ledong and Dongfang districts were interpreted and identified. Through the seismic layer flattening method, the seismic data volume was flattened along the seismic reflection layer corresponding to the specific geological interface, thereby reconstructing the ancient landform and restoring the paleogeomorphology of the Huangliu Formation. The thickness map and instantaneous amplitude map were based on seismic time-to-depth conversion and attribute extraction technology to analyze and display the distribution patterns of the channels and the lobes as well as lithology variation.

4. Results

4.1. Well Logging-Core-Thin Section Observation

In the Dongfang area, logging is mainly characterized by medium- to high-amplitude bell- or box-shaped curves that have positive grain sequence features (Figure 3a). The sandstone of the Huangliu Formation in Well DF-a is mainly fine to very fine sandstone with particle diameters distributed in the range of 0.120–0.040 mm, and the maximum thickness of a single sand body is 37 m. The core image (Figure 3a) shows light gray massive bedding and parallel bedding features. Based on the thin section analysis of Well DF-a sediment and other Dongfang sediment slices (Figure 3c), the detrital compositions consist of quartz (average 61%), potassium feldspar (average 3%) and other rock debris (average 9.5%), with medium sorting and subrounded roundness. The quartz comprises a large amount of monocrystalline quartz (55%) and a small amount of polycrystalline quartz (6%). The rock debris contains mainly metamorphic rocks (average 9%), and the content of the argillaceous matrix is relatively low (1%).

The well logging curves in the Ledong district are predominantly box-shaped, with an abrupt interface between the sandstone and mudstone at ca. 4045 m. (Figure 3b). The lithology of the Huangliu Formation in Well LD-b is mainly medium sandstone, with locally developed fine sandstone, and the maximum thickness of a single sand body can reach 36 m. Through core observation (Figure 3b), typical gravity flow sedimentary structures, such as massive bedding, Bauma sequences and mud gravel, can be identified. The massive sandstone contains apparent gravel and is poorly sorted. The results of the rock thin section analysis (Figure 3d) in Well LD-b show that the grain diameters are mainly distributed in the range of 0.500–0.050 mm, with poor sorting and subangular roundness. The average contents of monocrystalline quartz, polycrystalline quartz, potassium feldspar, plagioclase and rock debris are 58%, 20%, 7%, 3% and 1%, respectively. The rock debris is mainly composed of intrusive rocks.

The above logging-core-thin section observation (Figure 3) results present the most representative results among 23 logging curves, 160 m core and 129 thin sections. The results of the drilling and core data not shown in the paper are similar to the above given data.

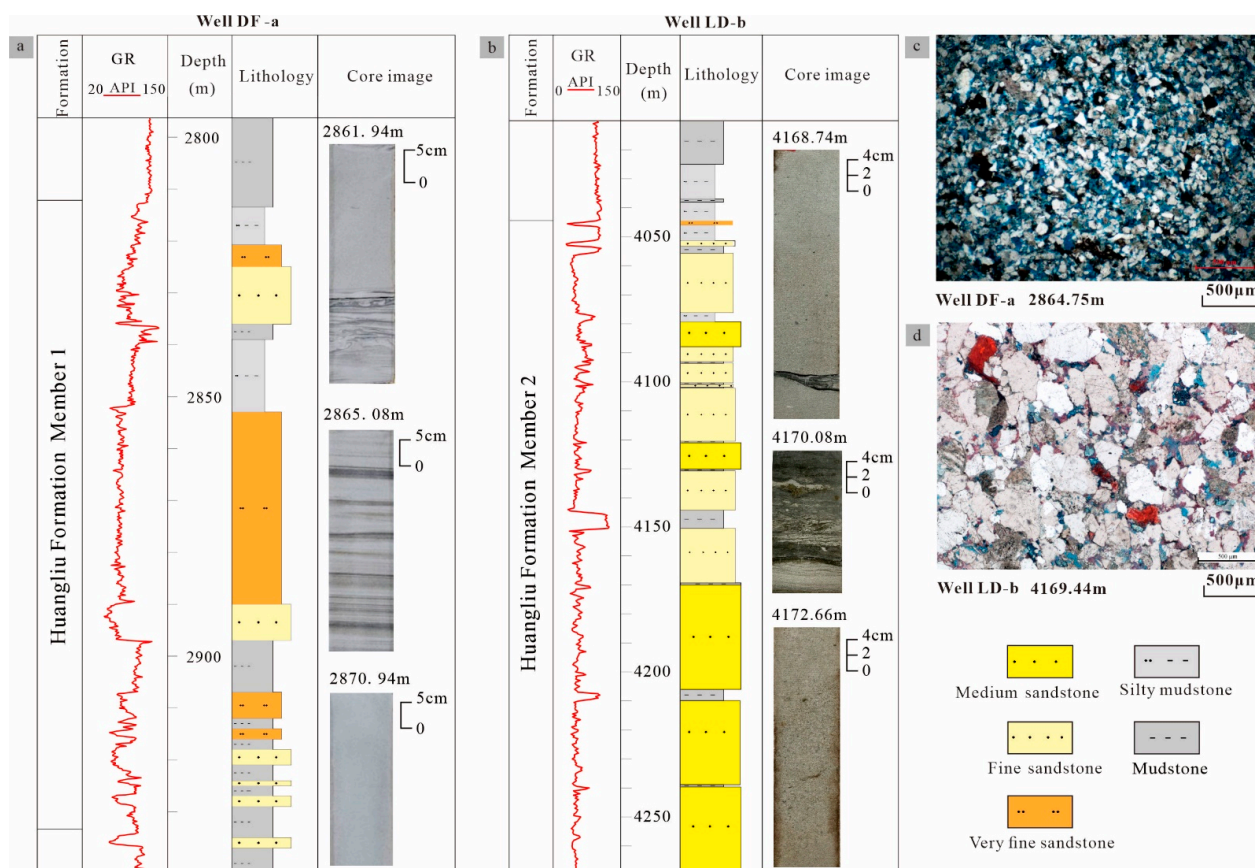


Figure 3. Well logging curves, lithology interpretation, core images and thin section observations: (a) Well DF-a in the Huangliu Formation upper member. (b) Well LD-b in the Huangliu Formation lower member. (c) Well DF-a sample thin section observation at 2864.75 m. (d) Well LD-b sample thin section observation at 4169.44 m.

4.2. Heavy Mineral Assemblage and Zircon U-Pb Dating

The heavy mineral assemblage results (Figure 4) of drilling samples from the Dongfang block demonstrate that leucoxene (average 65.85%), zircon (average 7.24%) and tourmaline (average 10.47%) dominate in the Dongfang wells, with an average ZTR index of 19.68. Drilling samples from the Ledong block wells display high contents of magnetite (30.54%), zircon (average 28.20%), tourmaline (average 14.65%) and garnet (average 11.73%), with an average ZTR index of 40.86. The fluvial sand samples from Hainan Island are dominated by zircon (average 27.73%), garnet (average 16.47%) and magnetite (average 20.44%), with an average ZTR index of 41.46. The river sands of eastern Vietnam and the Red River are dominated by leucoxene (average 42.33%), zircon (average 12.83%), rutile (average 15.56%), garnet (average 13.86%) and titanite (average 12.36%), with an average ZTR index of 28.39.

The zircon U-Pb dating spectra of both the Hainan river sand samples and the Ledong channel sediment samples (Figure 5) show bimodal characteristics, containing the main peaks of two geological ages: Cretaceous (97–99 Ma) and Permian–Triassic (232–249 Ma), respectively. The Cretaceous peaks are higher in the Ningyuan and Wanglou Rivers of Hainan Island, and the Permian–Triassic peaks are higher in the Changhua River of Hainan Island. The two peaks of the Ledong samples are similar in height, and some small Jurassic (151–153 Ma) peaks occur. The zircon dating patterns of the river sands, having northwestern provenance and the rock cuttings of the Huangliu Formation from the Dongfang submarine fan, display multiphase patterns. Among these, the samples from the Red River, Lam River, Ma River and the Dongfang block have distinct Paleogene (30–37 Ma), Permian–Triassic (243–262 Ma) and Silurian–Devonian (420–456 Ma) peaks, whereas the Giang River has significant Triassic peaks (248 Ma).

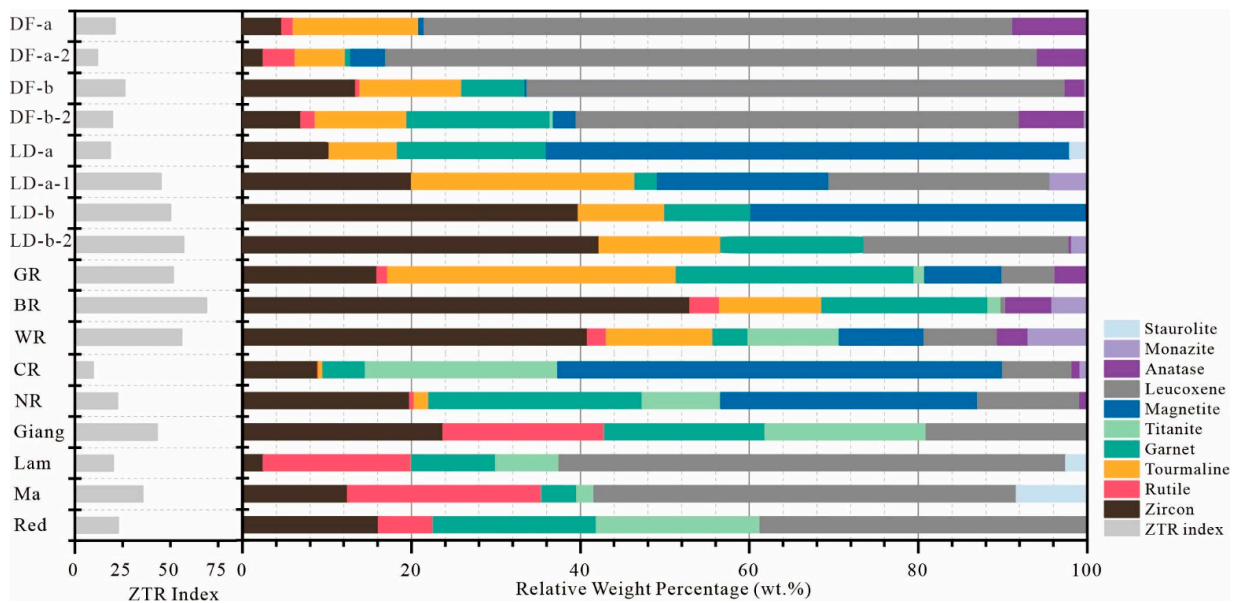


Figure 4. Heavy mineral assemblage and zircon–tourmaline–rutile (ZTR) index ratios of present-day fluvial sand samples, Ledong borehole samples and Dongfang borehole samples. The northwestern provenance data, such as that from the Giang River, Lam River, Ma River and Red River sands, were abstracted from Fyhn et al. (2019) [44].

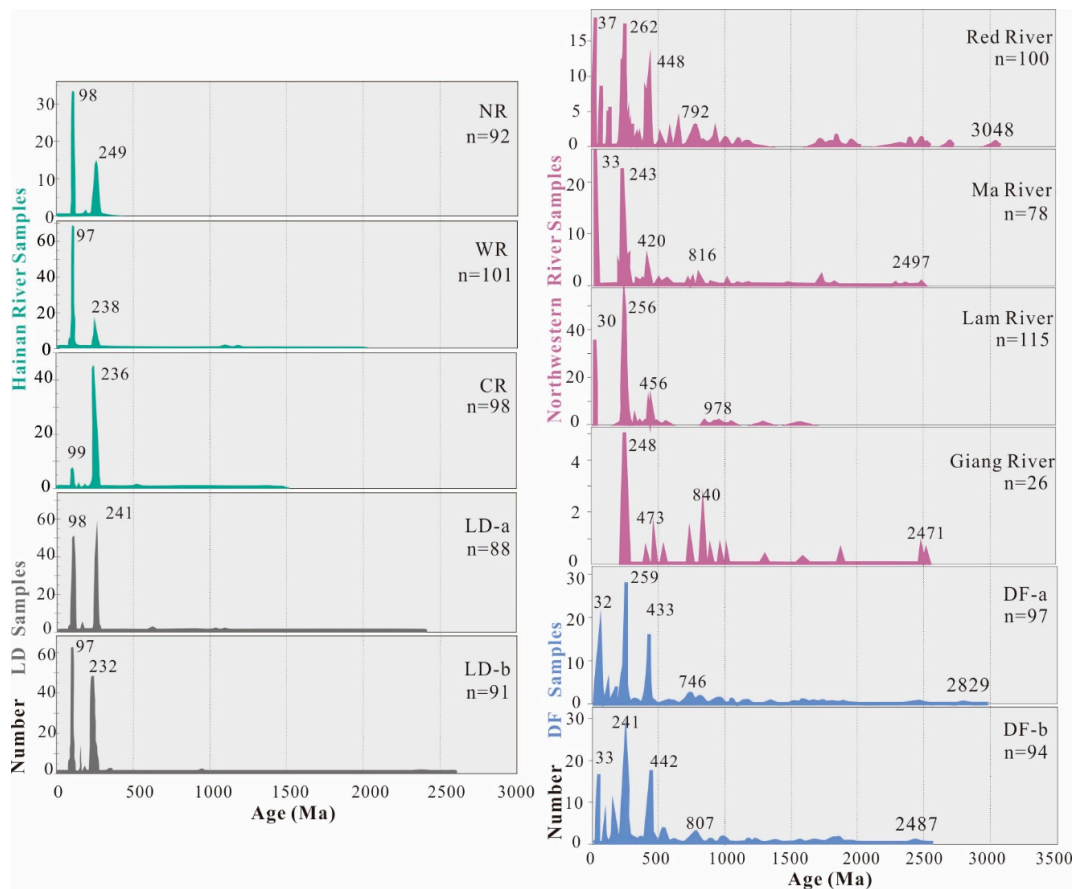


Figure 5. Detrital zircon Pb206/U238 age spectrum of Hainan River samples (green), Ledong samples (gray), northwestern river samples (purple) and Dongfang samples (blue). The “n” denotes the total number of zircons used for dating.

The result of the heavy mineral composition and zircon U-Pb geochronology of the selected four samples collected in this paper are typical and representative, which can provide a reliable basis for the study of sources in the two regions. Some scholars have previously made geochemical analyses on the sediments of the Huangliu Formation in the Dongfang district and Ledong district, and the findings reflected by the previous results are consistent with the results of the sampling analysis in this paper [21,22,36,37].

4.3. Seismic Processing

The seismic results show that the Dongfang fan developed in the northwest Central Depression in a flexure zone near the mud diapir, and it was distributed in a lenticular form between seismic interfaces T31 and T30 (Figure 6a). It is a composite submarine fan formed by the superposition of multistage lobes and channels. The topography of the Dongfang region in the late Miocene was relatively gentle and flat (Figure 6b), with slopes ranging between 2 to 3.2 degrees near well DF-b and 5.6 to 8 degrees near well DF-a.

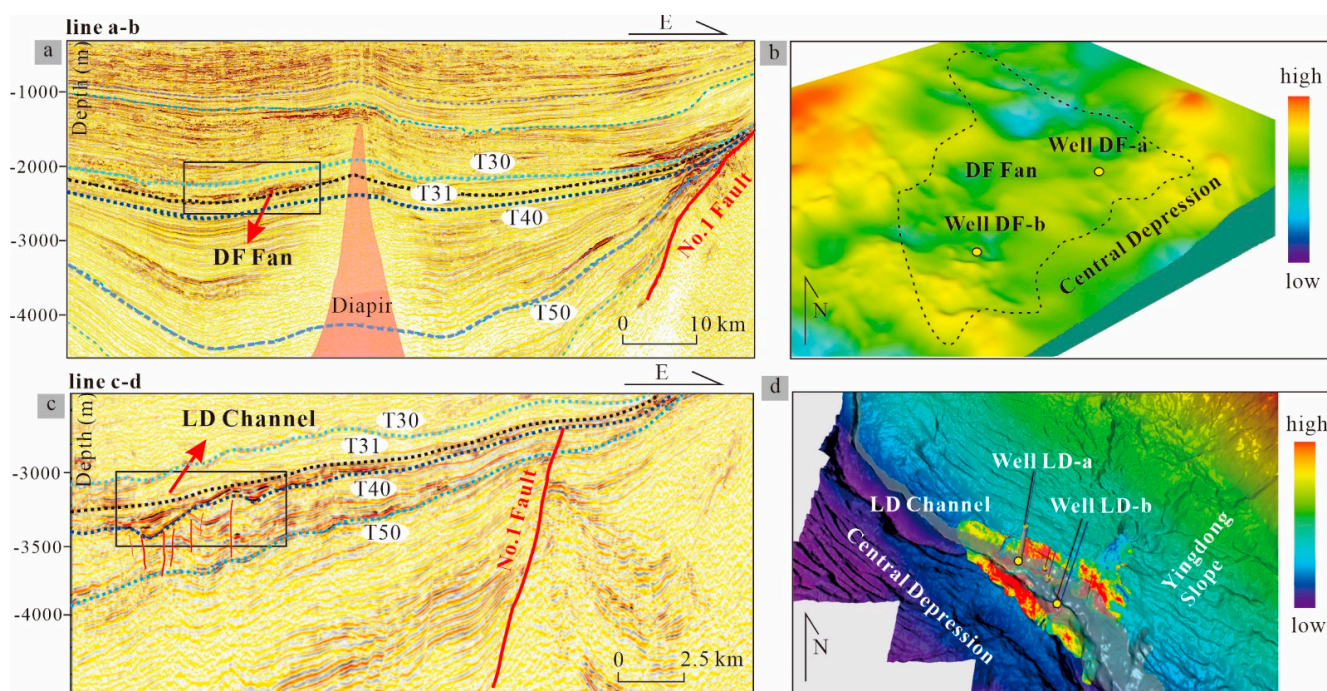


Figure 6. Seismic profiles and regional palaeotopography restorations (see the locations of lines a-b and c-d in Figure 1): (a) Seismic profile of the Dongfang fan developed in the second member of the Huangliu Formation between T30 and T31. (b) Dongfang Block palaeotopography restoration. (c) Seismic profile of the Ledong channel developed in the first member of the Huangliu Formation between T31 and T40. (d) Ledong Block palaeotopography restoration.

The Ledong channel, which developed under the No. 1 Fault slope break zone of the Yingdong Slope, is located between seismic interfaces T40 and T31 (Figure 6c). The bottom interface of the channel is U-shaped or V-shaped, with strong amplitude and high continuity. Several small hidden faults developed at the channel bottom. The paleogeomorphic restoration shows that, in the late Miocene Huangliu Formation, the terrain from Yingdong Slope to the Central Depression was steep (Figure 6d), with slopes near Well LD-a and Well LD-b that were both greater than 15 degrees.

According to the seismic reflection interfaces, the contact relationship between the sedimentary strata and the distribution of the sand layer, the submarine channel and the submarine fan sand body are divided into two stages. The first-stage sand body is located at the bottom of the gravity flow and was formed earlier, whereas the second-stage sand body is located above the first-stage sand body and was formed later. The sand thickness map shows that, in the early stage of submarine fan development (Figure 7a), the reservoir

mainly developed on the southwestern side, and the average thickness of the lobe is 38 m. In the later stage of the development of the submarine fan (Figure 7b), the fan area retreated to the northwest with decreased average thickness (30 m) and more evident channelization. The instantaneous amplitude map (Figure 7c,d) shows that the Ledong channel consists of two upstream tributaries in the northwest and northeast and one downstream tributary in the southeast, distributed in a “Y” shape. The sand reservoir in the first stage of channel development shows high continuity and connectivity along the channel. In the second stage of channel development, the sediment mud content increased, showing a strip with a small width on the plane.

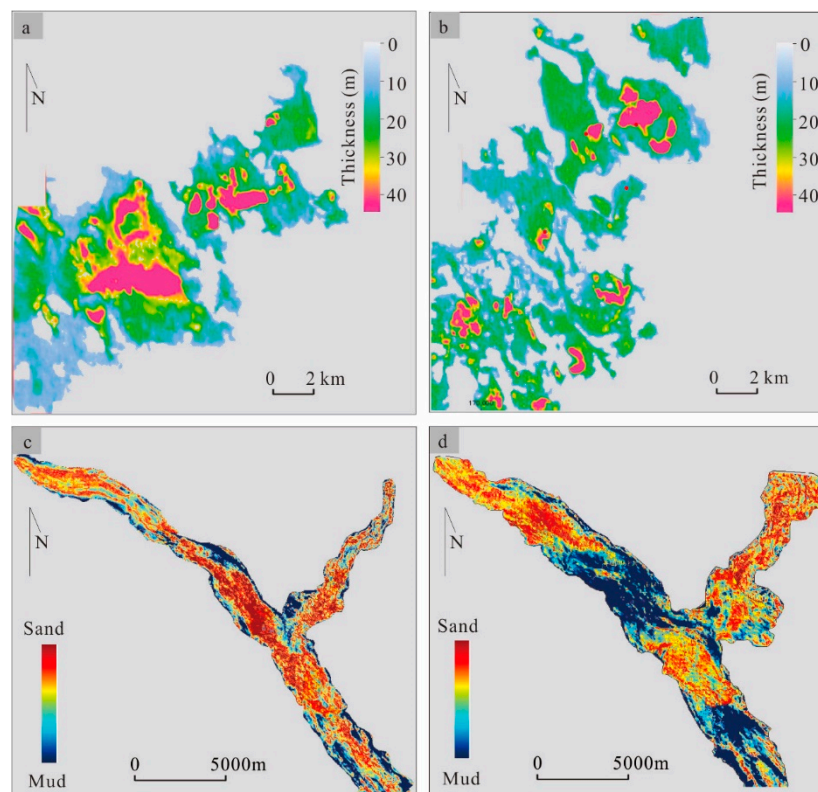


Figure 7. Thickness maps and instantaneous amplitude maps: (a) Thickness map of the Dongfang submarine fan developed in the first stage. (b) Thickness map of the Dongfang submarine fan developed in the second stage. (c) Instantaneous amplitude map of the Ledong submarine channel developed in the first stage. (d) Instantaneous amplitude map of the Ledong submarine channel developed in the second stage.

5. Discussions

5.1. Provenance Comparison

The combination of data from logging, cores, thin-section microscopic observations, heavy mineral analyses and zircon dating indicates that the provenances of the studied areas have different sources. Specifically, the Dongfang submarine fan sedimentary system developed in the Miocene Huangliu Formation is from the northwestern margin of the Yinggehai Basin, and the source of the Ledong channel sedimentary system, which developed in the same geological period, is from the eastern margin of the basin.

The maturity of the rock structure in the Ledong area is higher than that in the Dongfang area, suggesting that the transportation distance of provenance in the Dongfang area is longer than that in the Ledong area. The clastic particles from the Dongfang Fan exhibit high rock structure maturity with smaller particle sizes (0.120–0.040 mm versus 0.5–0.050 mm), high roundness and good sorting when compared with samples from the Ledong channel, indicating that the overall particle transport distance was longer [50,51].

In contrast, the Ledong sandstone is poorly sorted with a larger particle size than the Dongfang sandstone. Gravels in massive sandstone are often observed in the Ledong core sections. The Ledong rock structure maturity is low, reflecting features of near-source accumulation. The lengths (average 487 km) and drainage areas (average 80,000 km²) of rivers from the northwestern provenance, such as the Red River and Lam River, are larger than those of the rivers of Hainan Island, and the distance required for transportation from the source to the sedimentation area was longer [36,52] (Figure 1a). Therefore, the source of the Dongfang region more likely originated from the northwestern provenance.

The rock composition study suggests that the Ledong provenance is more likely to have originated from Hainan Island, which is rich in magmatic rocks. Both the Ledong and Dongfang sandstone compositions are dominated by quartz, feldspar and rock debris (Figure 3). The Ledong rock debris is mainly composed of intrusive rocks. In contrast, the Dongfang rock debris contains mainly metamorphic rocks (average 9%), and the content of the argillaceous matrix is relatively low (1%), reflecting higher maturity of the rock composition and longer particle transport distance characteristics [50,53]. The most significant difference lies in the content of polycrystalline quartz. The content of polycrystalline quartz in the Ledong sample slices (20%) is higher than that in the Dongfang samples (6%). Researchers have found that polycrystalline quartz grains with similar sizes, sub-equiaxial morphologies and non-oriented arrangement characteristics are most likely derived from granite [54]. The polycrystalline quartz grains found within the thin Ledong sections have shown the above features and are mostly contacted by sutures, reflecting a granite origin. Compared with the Yangtze plate and the Indian Plate, Hainan Island's magmatic rocks are widely distributed (Figure 2), with an exposed area of approximately 17,000 km², covering 45% of the whole island [55]. Mesozoic–Paleozoic granites are mainly developed on the central and southern islands, and a large number of Cenozoic basalts appear in the north. These magmatic rocks were mainly formed during the Hercynian–Indosinian period, when volcanic magmatism was frequent and intense [45]. Therefore, the Ledong source is more likely to have Hainan provenance.

With respect to heavy mineral assemblage (Figure 4), the Dongfang well samples are more similar to the Lam, Ma, Giang and Red River samples, which are characterized by high leucoxene, low zircon and low ZTR values. The northwestern provenance presents relatively low maturity of heavy minerals (ZTR% 28.39), as fewer magmatic parent rocks are exposed in eastern Vietnam and the southern Yangtze plate (Figure 2), accounting for approximately 5% [41], so the zircon content from the northwestern provenance is lower than that from the Hainan provenance. The Ledong well samples are more similar to Hainan rivers, such as the Ningyuan, Wanglou, Changhua, Ganen and Beili Rivers, which are characterized by having high zircon, high magnetite, high garnet, high ZTR and low leucoxene values (Figure 4). The Hainan provenance has a high degree of maturity of heavy minerals (ZTR 41.46%). The abundant zircon and magnetite in the Hainan River sands come from the intermediately acidic granites exposed on the island [32].

Since the Miocene, the sediment compositions provided by the rivers around the Yinggehai Basin have not remained exactly constant but have been influenced by tectonics, weathering and other factors [2,56,57]. However, in this research, we sampled the modern river deposits to compare with the Miocene (ca. 8.2–5.3 Ma) sediments in the basin from the wells based on the assumption that the rivers around Yinggehai Basin had a similar detrital zircon signature in the Miocene as they do at present. This assumption is based on the following evidence. Since the late Miocene, no large-scale plate collision or river capture events have been recorded [7]. After the collision of the Indosinian–Eurasian plate and the uplift of the Qinghai–Tibet orogenic belt in the late Paleocene to early Eocene, the provenance characteristics of the Yangtze plate, Indosinian plate and South China plate have been relatively stable [40,58]. Previous research has found that the Red River was captured by the Yangtze River before the late early Miocene [37]. However, since the late Miocene, no such large-scale river change events have occurred in the surrounding basins of Yinggehai basin. In addition, many scholars have also used modern river samples to

replace specific ancient river samples when studying the provenance of Yinggehai basin, which has been proved to be a reliable way [21,36]. Therefore, river sediments around the Yinggehai Basin have maintained relatively stable geochemical characteristics, and the age distribution of river sediments in the late Miocene is similar to that of modern river sediments.

The zircon U-Pb dating results are well matched with that of the lithological distribution in the source area. The lithologies exposed in the Yangtze block and the Indo-China block in the northwestern part of the basin are relatively complex, ranging from Cenozoic to Archaean strata [24,59] (Figure 2). Therefore, the Lam, Ma, Giang and Red Rivers are characterized by multiple high Cenozoic (33–37 Ma), Mesozoic (243–262 Ma) and Paleozoic (420–456 Ma) peaks and by multiple low Proterozoic peaks, such as 735–1028 Ma, 1700–1853 Ma and 2471–2490 Ma (Figure 5), mainly from Paleoproterozoic, Meso-Neoproterozoic deep metamorphic rocks and Meso-Neoproterozoic volcanic rocks from the northwestern provenance [44,60]. Cretaceous strata are widely distributed in the southwestern Hainan Island, and Permian to Triassic granites are largely exposed in the northwestern Hainan Island, with only a few Mesozoic to Paleozoic strata remaining in island blocks in the granite zone throughout the island [21]. Therefore, the Hainan provenance has two distinct peaks: Cretaceous and Permian–Triassic (Figure 5). The Cretaceous peaks are more prominent in the Ningyuan and Wanglou Rivers, which are located on the southwestern margin of Hainan Island, whereas the Permian–Triassic peaks are more prominent in the Changhua River on the northwestern margin of Hainan Island (Figure 5). It can be intuitively seen from the MDS diagram that the characteristics of the Hainan provenance and the northwestern provenance are clearly distinguished (Figure 8). The zircon age signatures of sandstone samples from Well LD-a and Well LD-b are closely linked to the Hainan provenance, whereas the Well DF-a and Well DF-b sandstone samples are adjacent to the northwestern provenance.

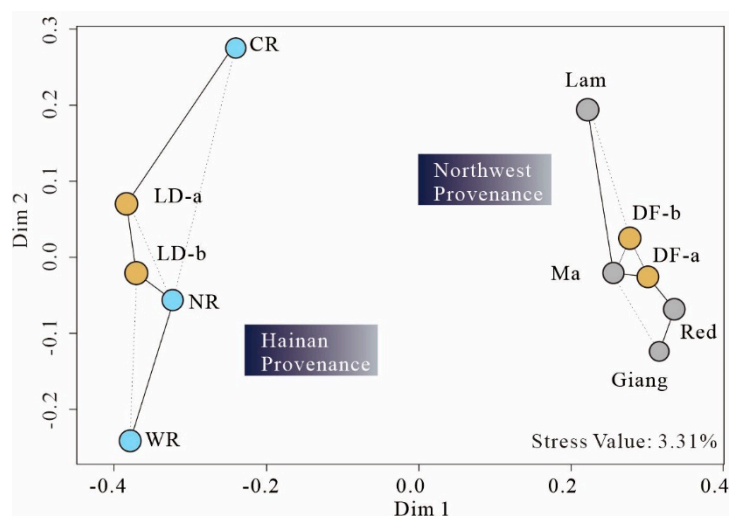


Figure 8. Multidimensional scaling (MDS) plot of detrital zircon U-Pb ages in river and study block sediments. The distance between samples was positively correlated with the Kolmogorov–Smirnov dissimilarity of their dating data. The solid lines connect the nearest neighbors, and the dotted lines link the second nearest samples. The stress value of 3.31% demonstrates an acceptable goodness of fit. The yellow, blue and gray dots represent the borehole samples, Hainan River samples and northwestern river samples, respectively.

5.2. Route to Source Comparison

A previous study found that the majority of continental-margin deep-water depositions occurred during periods of low sea levels [2]. The relative sea level decline was one of the most important factors triggering the development of marine gravity-driven systems in the basin during the Miocene [57,61]. The large-scale sea-level decline in the

early depositional stage of the Huangliu Formation in the South China Sea has been confirmed by paleontological and geochemical evidence [56]. This feature is consistent with global sea-level changes (Figure 1b). In the early Miocene, when the sea level rose and accommodation space increased, deltas were extensively developed around the basin on the continental shelf due to continuous feeding from provenance rivers [38,60] (Figure 9a). The Yinggehai Basin strata experienced several relative sea level declines during the deposition process, among which the relative sea level declined sharply at the beginning of the late Miocene Huangliu Formation, and this decline was the largest in all geologic periods (Figure 1b), which was conducive to the transport of deltaic sediments along the land slope and the formation of gas reservoir deposits in the basin [22,62]. The Central Canyon in the Qiongdongnan Basin of the South China Sea and the second phase of the Bengal–Nicobar Fan in the Bay of Bengal were also initially developed ca. 10.5 Ma [1,63]. The thickness and connectivity of the sand body in the first stage are better than those in the second stage, during which the sea level gradually rose (Figure 7). Typical gravity flow deposition structures, such as the Bouma sequence, massive bedding and deformed bedding structures, can be observed (Figure 3) in both core sections. Multiple sets of thick sand body reservoirs are sandwiched between mud layers in both the Ledong and Dongfang wells, and the lithology fines upward (Figure 3), reflecting that the overall hydrodynamic conditions have changed from strong to weak [4,27].

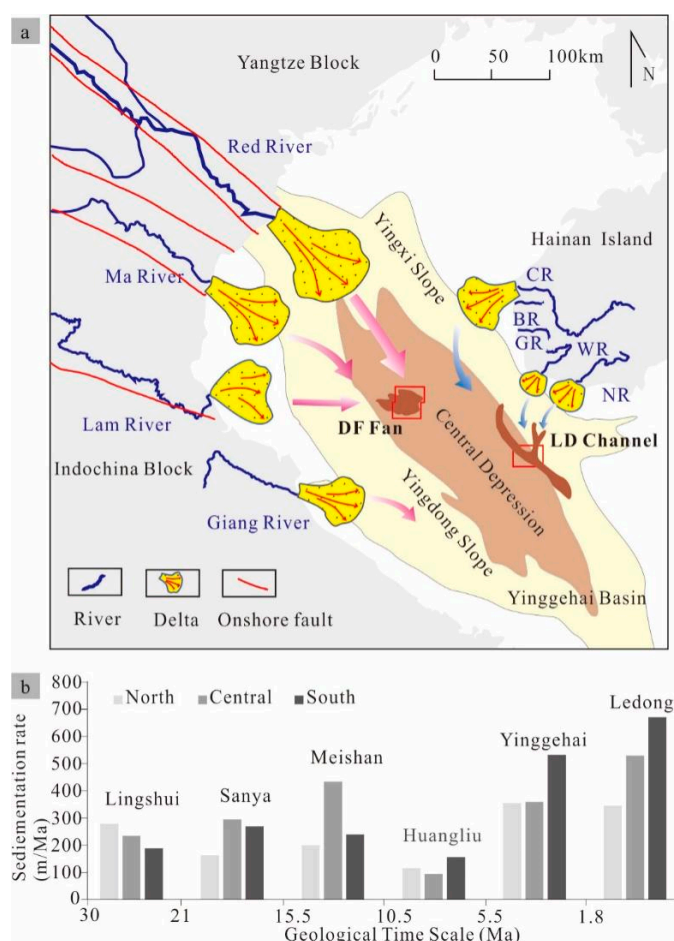


Figure 9. (a) Late Miocene sedimentary model for the Ledong submarine channel and Dongfang submarine fan in the Yinggehai Basin Huangliu Formation. The red arrow indicates northwestern provenance migration, whereas the blue arrow indicates Hainan provenance migration. NR: Ningyuan River, WR: Wanglou River, GR: Ganen River, BR: Beili River, CR: Changhua River. (b) Yinggehai Basin sedimentation rate in the northern, central and southern regions (data modified from Liu et al. (2017) [64]).

The source transport pathways of paleorivers are not very different from those of modern rivers. In the Miocene, the fault zone around the basin controlled the development of the paleotectonic “trench” and provided a path for the transportation of the provenance [64]. The Yingxi Fault zone, consisting of the Da River Fault, Lam River Fault, Ma River Fault and Troung Son Fault, strikes in the SSE–SE direction [30] (Figure 2). The Red River fault zone in the Yinggehai Basin strikes in the near-SN direction [60]. The paleotectonic “trenches” are well developed under the control of these two major fault zones. For example, the paleo Red River, Ma River and Lam River trenches are well superimposed (Figure 9a) with the Red River Fault, Ma River Fault and Lam River Fault, with an SSE–SE striking direction as well [64]. Therefore, the Yingxi Fault zone and the Red River Fault zone controlled the development and trends of ancient rivers. The ancient and modern Red River, Ma River and Lam River all developed along the SSE–SN fault zone [65,66].

Since ca. 30 Ma, the sedimentary center of the Yinggehai Basin migrated from northwest to southeast [26,38]. In the late Miocene Huanliu Formation, the sedimentation center was in the southern part of the basin, which prompted southeastward gravity flow deposition, as shown in Figure 9b. The migration is evidenced by the changes in sedimentation rate in the basin from the Oligocene to the present [67]. During the late Oligocene (30–21 Ma), the sedimentary center of the basin was located in the Lingao area in the north, with a deposition rate of 278 m/Ma (Figure 9b). The depositional center migrated to the central region in the early Miocene Sanya Formation to Meishan Formation deposition period (21–10.5 Ma), with increasing deposition rates of 294 m/Ma and 433 m/Ma, respectively. During the deposition of the Miocene Huangliu Formation, the deposition rate in the south gradually exceeded the deposition rate in the center, and the deposition center began to migrate further southward with a relatively low sedimentation rate of 155 m/Ma [67]. From the deposition period of the Pliocene Yinggehai Formation to the Ledong Formation (5.5 Ma—present), the deposition rate of the southern area increased rapidly, reaching 531 to 670 m/Ma.

The gravity flow systems developed in the study areas of Ledong and Dongfang are also greatly influenced by regional tectono-morphologic factors, such as regional faulting activities, in situ paleotopography and the style of slope break belts developed on the continental margin. During the depositional period of the Huangliu Formation, the paleogeomorphic environment and the circumferential tectonic activity in the Ledong and Dongfang regions had a clear controlling role on the formation, evolution, development and spatial distribution characteristics of the sedimentary systems. The submarine channel developed in the eastern part of the basin is mainly affected by the faulted slope break zone controlled by the No. 1 Fault zone, and the submarine fan in the western part of the basin is affected by the flexure slope break zone controlled by the Yingxi Fault zone (Figure 10). The violent movement of the No. 1 Fault led to regional tectonic subsidence and the formation of a faulted slope break belt on the eastern margin of the basin [6,28]. The Yingdong Slope in the east of the basin is dominated by the No. 1 Fault, with a high level of faulting activity. The average activity rates of the southern section of the No. 1 Fault in the Sanya Formation (21–15.5 Ma), early Meishan Formation (15.5–13.4 Ma), late Meishan Formation (13.4–10.5 Ma), early Huangliu Formation (10.5–8.2 Ma) and late Huangliu Formation (8.2–5.5 Ma) are approximately 49, 57, 78, 35 and 46 m/Ma, respectively [68]. The faulted slope break belt has a high slope–fall ratio (Figure 10), and the fault-descent plate forms a certain sedimentary slope toward the center of the basin. Thus, the paleomorphological slope of the Ledong district is relatively steep, which easily triggers the development of gravity flow along the clinoform [69]. At the same time, hidden faults are traced under the T40 seismic interface at the bottom of the Ledong channel (Figure 6c), making the strata in this area more susceptible to the later transformation of terrigenous debris and currents to form a gravity flow channel. Therefore, the development of the northwestern trend tributary path is restricted by the low terrain created by the southeastern trend bottom faults, and the northeastern trend tributary sediment transportation route is along the faulted slope break. The Yingxi Fault zone in the western part of the basin is controlled by

several medium- to small-scale normal faults (Figure 10), with average slopes ranging from 3° to 5° , among which the first-level flexural slope break is controlled by some medium faults, such as the Lam River fault, Ma River fault and Da River Fault [26]. This geomorphic feature makes the distribution of the sedimentary system to be mainly controlled by the rise and fall of sea level, the location of slope break points and the migration of the deposition center. During the late Miocene, the deposition center was in the southeastern part of the basin, and the paleogeomorphic slope in the Dongfang area tended to be gentle, leaning steadily toward the SSE direction. The SSE-trending Dongfang submarine fan sedimentary system developed in the open and flat area.

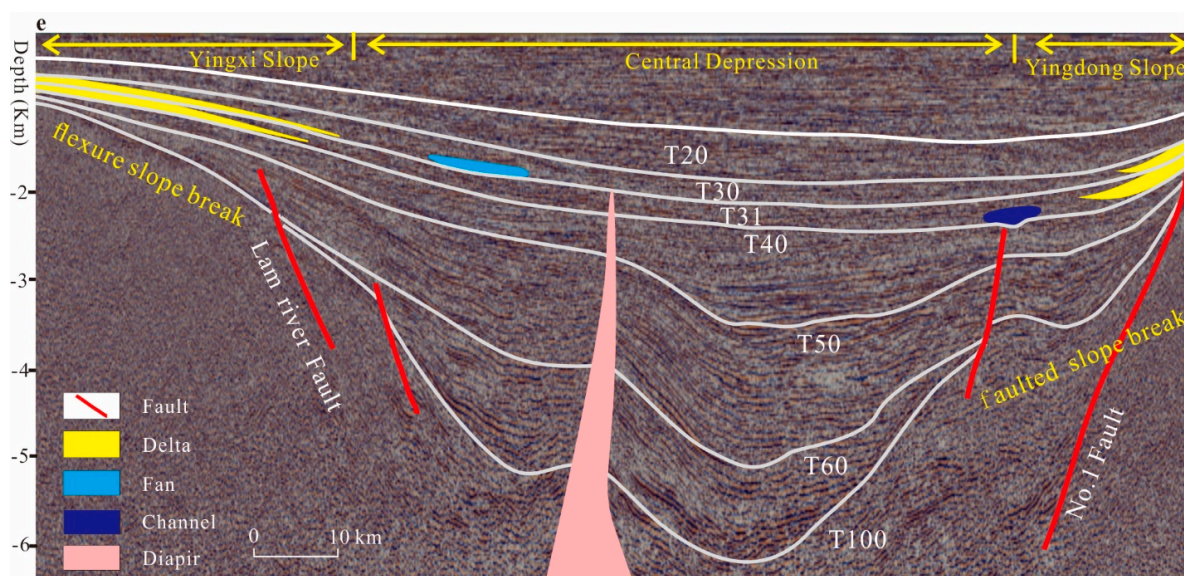


Figure 10. The flexure slope break zone was controlled by the Yingxi fault zone in the western margin of the basin, and the faulted slope break zone was controlled by the No. 1 Fault zone in the eastern margin of the basin (see the location of lines e–f in Figure 1).

6. Conclusions

From the perspective of source-to-sink, this study comparatively analyzed the provenance sources, formation mechanisms and sedimentary characteristics of the late Miocene axially restricted channel in the Ledong district and the submarine fan in the Dongfang district. The unique regional tectonic pattern of the Yinggehai Basin and the abundant source supplies are the dominant factors in the formation of the gravity flow source-to-sink sedimentary system and gas reservoirs in the study area. The sedimentary systems were generally influenced by the coupling control of sea level decline in the Miocene and the high-north low-south paleomorphology, which facilitated the debris migration into the basin and southward transport. The existence of a slope break zone in the margin of the basin promoted the formation of continuing gravity flows that were unloaded near the deposition center. In addition, the spatial variations within the basin controlled the deposition processes.

The source supply of the Ledong channel on the Yingdong Slope had Hainan provenance from the eastern part of the basin. With a short sediment transport distance, the rock structure is less mature, and the content of polycrystalline quartz in the rock composition is relatively high, showing a magmatic genesis. The heavy mineral assemblages are marked by high zircon, high ZTR and low leucoxene values. The zircon U-Pb age is characterized by the bimodal form of Cretaceous and Permian–Triassic peaks. The eastern margin slope break was affected by higher faulting intensity in the southern section of the No. 1 Fault and developed a faulted slope break zone characterized by relatively large and steep slopes, creating a favorable transport pathway for the rapid deposition of deltaic sands. The

regional hidden fracture zone built up a natural low topography for the development of restricted channels.

The Dongfang submarine fan located in the Central Depression was fed by rivers in the northwestern margin of the basin, including the Red River and the rivers of eastern Vietnam. The Dongfang sediments were transported over long distances and present a higher maturity of rock structure than the Ledong sediments. The heavy minerals are characterized by high leucoxene, low zircon and low ZTR. Zircon age spectra show a multi-peak coexistence. Affected by the Yingxi fault zone, the northwestern margin of the basin developed several normal faults and formed a gently sloping flexure slope break belt. When the sea level dropped, the debris was transported through the flexural slope break belt to the relatively flat and open area below the break point and was deposited to form a seafloor fan tilting to the SSE.

Author Contributions: Conceptualization, investigation and data curation, Y.Y. and Q.G.; methodology, Q.G. and H.W.; formal analysis, validation, software, resources and visualization, Y.Y.; writing—original draft preparation, Y.Y. and Q.G.; writing—review and editing, Y.Y. and H.W.; supervision, H.W.; project administration and funding acquisition, H.W. and Q.G. All authors have read and agreed to the published version of the manuscript.

Funding: This research was funded by the Key Program of the National Natural Science Foundation of China (grant numbers U19B2007) and the scholarship of China Postdoctoral Foundation (grant numbers 2021M700201).

Institutional Review Board Statement: Not applicable.

Informed Consent Statement: Not applicable.

Data Availability Statement: Not applicable.

Acknowledgments: The authors would like to acknowledge the China National Offshore Oil Corporation (Haikou and Zhanjiang Branch).

Conflicts of Interest: The authors declare no conflict of interest.

References

1. Gong, C.; Steel, R.J.; Qi, K.; Wang, Y. Deep-Water Channel Morphologies, Architectures, and Population Densities in Relation to Stacking Trajectories and Climate States. *Bull. Geol. Soc. Am.* **2020**, *133*, 287–306. [[CrossRef](#)]
2. Covault, J.A.; Graham, S.A. Submarine Fans at All Sea-Level Stands: Tectono-Morphologic and Climatic Controls on Terrigenous Sediment Delivery to the Deep Sea. *Geology* **2010**, *38*, 939–942. [[CrossRef](#)]
3. Shanmugam, G. Deep-Marine Tidal Bottom Currents and Their Reworked Sands in Modern and Ancient Submarine Canyons. *Mar. Pet. Geol.* **2003**, *20*, 471–491. [[CrossRef](#)]
4. Shanmugam, G. *Submarine Fans: A Critical Retrospective (1950–2015)*; Elsevier Ltd.: Amsterdam, The Netherlands, 2016; Volume 5, ISBN 3695110139.
5. Yu, K.; Miramontes, E.; Alves, T.M.; Li, W.; Liang, L.; Li, S.; Zhan, W.; Wu, S. Incision of Submarine Channels Over Pockmark Trains in the South China Sea. *Geophys. Res. Lett.* **2021**, *48*, e2021GL092861. [[CrossRef](#)]
6. Sun, M.; Wang, H.; Liao, J.; Gan, H.; Xiao, J.; Ren, J.; Zhao, S. Sedimentary Characteristics and Model of Gravity Flow Depositional System for the First Member of Upper Miocene Huangliu Formation in Dongfang Area, Yinggehai Basin, Northwestern South China Sea. *J. Earth Sci.* **2014**, *25*, 506–518. [[CrossRef](#)]
7. Wang, C.; Liang, X.; Xie, Y.; Tong, C.; Pei, J.; Zhou, Y.; Jiang, Y.; Fu, J.; Dong, C.; Liu, P. Provenance of Upper Miocene to Quaternary Sediments in the Yinggehai-Song Hong Basin, South China Sea: Evidence from Detrital Zircon U-Pb Ages. *Mar. Geol.* **2014**, *355*, 202–217. [[CrossRef](#)]
8. Gong, C.; Li, D.; Steel, R.J.; Peng, Y.; Xu, S.; Wang, Y. Delta-to-Fan Source-to-Sink Coupling as a Fundamental Control on the Delivery of Coarse Clastics to Deepwater: Insights from Stratigraphic Forward Modelling. *Basin Res.* **2021**, *33*, 2960–2983. [[CrossRef](#)]
9. Cathro, D.L.; Austin, J.A.; Moss, G.D. Progradation along a Deeply Submerged Oligocene-Miocene Heterozoan Carbonate Shelf: How Sensitive Are Clinoforms to Sea Level Variations? *Am. Assoc. Pet. Geol. Bull.* **2003**, *87*, 1547–1574. [[CrossRef](#)]
10. Fan, C.; Cao, J.; Luo, J.; Li, S.; Wu, S.; Dai, L.; Hou, J.; Mao, Q. Heterogeneity and Influencing Factors of Marine Gravity Flow Tight Sandstone under Abnormally High Pressure: A Case Study from the Miocene Huangliu Formation Reservoirs in LD10 Area, Yinggehai Basin, South China Sea. *Pet. Explor. Dev.* **2021**, *48*, 1048–1062. [[CrossRef](#)]
11. Duan, W.; Li, C.-F.; Chen, X.-G.; Luo, C.-F.; Tuo, L.; Liu, J.-Z. Diagenetic Differences Caused by Gas Charging with Different Compositions in the XF13 Block of the Yinggehai Basin, South China Sea. *AAPG Bull.* **2020**, *104*, 735–765. [[CrossRef](#)]

12. Huang, Y.; Tan, X.; Liu, E.; Wang, J.; Wang, J. Sedimentary Processes of Shallow-Marine Turbidite Fans: An Example from the Huangliu Formation in the Yinggehai Basin, South China Sea. *Mar. Pet. Geol.* **2021**, *132*, 105191. [[CrossRef](#)]
13. Huang, Y.; Kane, I.A.; Zhao, Y. Effects of Sedimentary Processes and Diagenesis on Reservoir Quality of Submarine Lobes of the Huangliu Formation in the Yinggehai Basin, China. *Mar. Pet. Geol.* **2020**, *120*, 104526. [[CrossRef](#)]
14. Craddock, W.H.; Kylander, A.R.C. U-Pb Ages of Detrital Zircons from the Tertiary Mississippi River Delta in Central Louisiana: Insights into Sediment Provenance. *Geosphere* **2013**, *9*, 1832–1851. [[CrossRef](#)]
15. Cerri, R.I.; Warren, L.V.; Varejão, F.G.; Marconato, A.; Luvizotto, G.L.; Assine, M.L. Unraveling the Origin of the Parnaíba Basin: Testing the Rift to Sag Hypothesis Using a Multi-Proxy Provenance Analysis. *J. S. Am. Earth Sci.* **2020**, *101*, 102625. [[CrossRef](#)]
16. Zhao, L.; Liu, X.; Yang, S.; Ma, X.; Liu, L.; Sun, X. Regional Multi-Sources of Carboniferous Karstic Bauxite Deposits in North China Craton: Insights from Multi-Proxy Provenance Systems. *Sediment. Geol.* **2021**, *421*, 105958. [[CrossRef](#)]
17. Caracciolo, L. Sediment Generation and Sediment Routing Systems from a Quantitative Provenance Analysis Perspective: Review, Application and Future Development. *Earth-Sci. Rev.* **2020**, *209*, 103226. [[CrossRef](#)]
18. Allen, P.A. From Landscapes into Geological History. *Nature* **2008**, *451*, 274–276. [[CrossRef](#)]
19. Liu, Z.; Zhao, Y.; Colin, C.; Statterger, K.; Wiesner, M.G.; Huh, C.A.; Zhang, Y.; Li, X.; Sompongchaiyakul, P.; You, C.F.; et al. Source-to-Sink Transport Processes of Fluvial Sediments in the South China Sea. *Earth-Sci. Rev.* **2016**, *153*, 238–273. [[CrossRef](#)]
20. Walsh, J.P.; Wiberg, P.L.; Aalto, R.; Nittrouer, C.A.; Kuehl, S.A. Source-to-Sink Research: Economy of the Earth's Surface and Its Strata. *Earth-Sci. Rev.* **2016**, *153*, 1–6. [[CrossRef](#)]
21. Cao, L.; Jiang, T.; Wang, Z.; Zhang, Y.; Sun, H. Provenance of Upper Miocene Sediments in the Yinggehai and Qiongdongnan Basins, Northwestern South China Sea: Evidence from REE, Heavy Minerals and Zircon U-Pb Ages. *Mar. Geol.* **2015**, *361*, 136–146. [[CrossRef](#)]
22. Jiang, T.; Cao, L.; Xie, X.; Wang, Z.; Li, X.; Zhang, Y.; Zhang, D.; Sun, H. Insights from Heavy Minerals and Zircon U-Pb Ages into the Middle Miocene-Pliocene Provenance Evolution of the Yinggehai Basin, Northwestern South China Sea. *Sediment. Geol.* **2015**, *327*, 32–42. [[CrossRef](#)]
23. Yao, Y.; Guo, S.; Zhu, H.; Huang, Y.; Liu, H.; Wang, X. Source-to-Sink Characteristics of the Channelized Submarine Fan System of the Huangliu Formation in the Dongfang Block, Yinggehai Basin, South China Sea. *J. Pet. Sci. Eng.* **2021**, *206*, 109009. [[CrossRef](#)]
24. Clift, P.D.; Sun, Z. The Sedimentary and Tectonic Evolution of the Yinggehai-Song Hong Basin and the Southern Hainan Margin, South China Sea: Implications for Tibetan Uplift and Monsoon Intensification. *J. Geophys. Res. Solid Earth* **2006**, *111*, 1–28. [[CrossRef](#)]
25. Li, X.; Wang, H.; Yao, G.; Peng, Y.; Ouyang, J.; Zhao, X.; Lan, Z.; Huang, C. Sedimentary Features and Filling Process of the Miocene Gravity-Driven Deposits in Ledong Area, Yinggehai Basin, South China Sea. *J. Pet. Sci. Eng.* **2021**, *209*, 109886. [[CrossRef](#)]
26. Wang, Z.; Xian, B.; Liu, J.; Fan, C.; Li, H.; Wang, J.; Zhang, X.; Huang, H.; Tan, J.; Chen, P.; et al. Large-Scale Turbidite Systems of a Semi-Enclosed Shelf Sea: The Upper Miocene of Eastern Yinggehai Basin, South China Sea. *Sediment. Geol.* **2021**, *425*, 106006. [[CrossRef](#)]
27. Huang, Y.; Yao, G.; Fan, X. Sedimentary Characteristics of Shallow-Marine Fans of the Huangliu Formation in the Yinggehai Basin, China. *Mar. Pet. Geol.* **2019**, *110*, 403–419. [[CrossRef](#)]
28. Xie, X.; Müller, R.D.; Ren, J.; Jiang, T.; Zhang, C. Stratigraphic Architecture and Evolution of the Continental Slope System in Offshore Hainan, Northern South China Sea. *Mar. Geol.* **2008**, *247*, 129–144. [[CrossRef](#)]
29. Ding, W.; Hou, D.; Zhang, W.; He, D.; Cheng, X. A New Genetic Type of Natural Gases and Origin Analysis in Northern Songnan-Baodao Sag, Qiongdongnan Basin, South China Sea. *J. Nat. Gas Sci. Eng.* **2018**, *50*, 384–398. [[CrossRef](#)]
30. Lei, C.; Ren, J.; Sternai, P.; Fox, M.; Willett, S.; Xie, X.; Clift, P.D.; Liao, J.; Wang, Z. Structure and Sediment Budget of Yinggehai-Song Hong Basin, South China Sea: Implications for Cenozoic Tectonics and River Basin Reorganization in Southeast Asia. *Tectonophysics* **2015**, *655*, 177–190. [[CrossRef](#)]
31. Qin, Y.; Alves, T.M.; Constantine, J.A.; Gamboa, D.; Wu, S. Effect of Channel Tributaries on the Evolution of Submarine Channel Confluences (Espírito Santo Basin, SE Brazil). *Bull. Geol. Soc. Am.* **2020**, *132*, 263–272. [[CrossRef](#)]
32. Gong, Y.; Pease, V.; Wang, H.; Gan, H.; Liu, E.; Ma, Q.; Zhao, S.; He, J. Insights into Evolution of a Rift Basin: Provenance of the Middle Eocene-Lower Oligocene Strata of the Beibuwan Basin, South China Sea from Detrital Zircon. *Sediment. Geol.* **2021**, *419*, 105908. [[CrossRef](#)]
33. He, J.; Garzanti, E.; Cao, L.; Wang, H. The Zircon Story of the Pearl River (China) from Cretaceous to Present. *Earth-Sci. Rev.* **2020**, *201*, 103078. [[CrossRef](#)]
34. Yang, J.; Huang, B. Origin and Migration Model of Natural Gas in L Gas Field, Eastern Slope of Yinggehai Sag, China. *Pet. Explor. Dev.* **2019**, *46*, 471–481. [[CrossRef](#)]
35. Fan, C. Tectonic Deformation Features and Petroleum Geological Significance in Yinggehai Large Strike-Slip Basin, South China Sea. *Pet. Explor. Dev.* **2018**, *45*, 190–199. [[CrossRef](#)]
36. Wang, C.; Liang, X.; Foster, D.A.; Xie, Y.; Tong, C.; Pei, J.; Fu, J.; Jiang, Y.; Dong, C.; Zhou, Y.; et al. Zircon U-Pb Geochronology and Heavy Mineral Composition Constraints on the Provenance of the Middle Miocene Deep-Water Reservoir Sedimentary Rocks in the Yinggehai-Song Hong Basin, South China Sea. *Mar. Pet. Geol.* **2016**, *77*, 819–834. [[CrossRef](#)]
37. Wang, C.; Liang, X.; Foster, D.A.; Tong, C.; Liu, P.; Liang, X.; Zhang, L. Linking Source and Sink: Detrital Zircon Provenance Record of Drainage Systems in Vietnam and the Yinggehai-Song Hong Basin, South China Sea. *Bull. Geol. Soc. Am.* **2019**, *131*, 191–204. [[CrossRef](#)]

38. Wang, C.; Liang, X.; Foster, D.A.; Liang, X.; Tong, C.; Liu, P. Detrital Zircon Ages: A Key to Unraveling Provenance Variations in the Eastern Yinggehai-Song Hong Basin, South China Sea. *Am. Assoc. Pet. Geol. Bull.* **2019**, *103*, 1525–1532. [[CrossRef](#)]
39. Chen, Y.; Zhang, D.; Zhang, J.; Huang, C.; Jiao, X.; Wang, Y. Sedimentary Characteristics and Controlling Factors of the Axial Gravity Channel in Huangliu Formation of the Yingdong Slope Area in Yinggehai Basin. *J. Northeast Pet. Univ.* **2020**, *44*, 91–102.
40. Yan, Y.; Carter, A.; Palk, C.; Brichau, S.; Hu, X. Understanding Sedimentation in the Song Hong-Yinggehai Basin, South China Sea. *Geochem. Geophys. Geosyst.* **2011**, *12*. [[CrossRef](#)]
41. Nguyen, H.H.; Carter, A.; Van Hoang, L.; Vu, S.T. Provenance, Routing and Weathering History of Heavy Minerals from Coastal Placer Deposits of Southern Vietnam. *Sediment. Geol.* **2018**, *373*, 228–238. [[CrossRef](#)]
42. Xie, Y.; Li, X.; Fan, C.; Tan, J.; Liu, K.; Lu, Y.; Hu, W.; Li, H.; Wu, J. The Axial Channel Provenance System and Natural Gas Accumulation of the Upper Miocene Huangliu Formation in Qiongdongnan Basin, South China Sea. *Pet. Explor. Dev.* **2016**, *43*, 570–578. [[CrossRef](#)]
43. Zhong, L.; Li, G.; Yan, W.; Xia, B.; Feng, Y.; Miao, L.; Zhao, J. Using Zircon U–Pb Ages to Constrain the Provenance and Transport of Heavy Minerals within the Northwestern Shelf of the South China Sea. *J. Asian Earth Sci.* **2017**, *134*, 176–190. [[CrossRef](#)]
44. Fyhn, M.B.W.; Thomsen, T.B.; Keulen, N.; Knudsen, C.; Rizzi, M.; Bojesen-Koefoed, J.; Olivarius, M.; Tri, T.V.; Phach, P.V.; Minh, N.Q.; et al. Detrital Zircon Ages and Heavy Mineral Composition along the Gulf of Tonkin—Implication for Sand Provenance in the Yinggehai-Song Hong and Qiongdongnan Basins. *Mar. Pet. Geol.* **2019**, *101*, 162–179. [[CrossRef](#)]
45. Pe-Piper, G.; Piper, D.J.W.; Wang, Y.; Zhang, Y.; Trottier, C.; Ge, C.; Yin, Y. Quaternary Evolution of the Rivers of Northeast Hainan Island, China: Tracking the History of Avulsion from Mineralogy and Geochemistry of River and Delta Sands. *Sediment. Geol.* **2016**, *333*, 84–99. [[CrossRef](#)]
46. Jiang, T.; Liu, X.; Yu, T.; Hu, Y. OSL Dating of Late Holocene Coastal Sediments and Its Implication for Sea-Level Eustacy in Hainan Island, Southern China. *Quat. Int.* **2018**, *468*, 24–32. [[CrossRef](#)]
47. Huang, B.; Xiao, X.; Hu, Z.; Yi, P. Geochemistry and Episodic Accumulation of Natural Gases from the Ledong Gas Field in the Yinggehai Basin, Offshore South China Sea. *Org. Geochem.* **2005**, *36*, 1689–1702. [[CrossRef](#)]
48. Andò, S.; Garzanti, E.; Padoan, M.; Limonta, M. Corrosion of Heavy Minerals during Weathering and Diagenesis: A Catalog for Optical Analysis. *Sediment. Geol.* **2012**, *280*, 165–178. [[CrossRef](#)]
49. Hubert, J.F. A Zircon-Tourmaline-Rutile Maturity Index and the Interdependence of the Composition of Heavy Mineral Assemblages with the Gross Composition and Texture of Sandstones. *SEPM J. Sediment. Res.* **1962**, *32*, 440–450. [[CrossRef](#)]
50. Garzanti, E. Petrographic Classification of Sand and Sandstone. *Earth-Sci. Rev.* **2019**, *192*, 545–563. [[CrossRef](#)]
51. Garzanti, E. From Static to Dynamic Provenance Analysis—Sedimentary Petrology Upgraded. *Sediment. Geol.* **2016**, *336*, 3–13. [[CrossRef](#)]
52. Milliman, J.D.; Farnsworth, K.L. *River Discharge to the Coastal Ocean: A Global Synthesis*; Cambridge University Press: Cambridge, UK, 2011; ISBN 9780511781247.
53. Baas, J.H.; Hailwood, E.A.; McCaffrey, W.D.; Kay, M.; Jones, R. Directional Petrological Characterisation of Deep-Marine Sandstones Using Grain Fabric and Permeability Anisotropy: Methodologies, Theory, Application and Suggestions for Integration. *Earth-Sci. Rev.* **2007**, *82*, 101–142. [[CrossRef](#)]
54. Wu, Y.; Zheng, Y. Genesis of Zircon and Its Constraints on Interpretation of U–Pb Age. *Chin. Sci. Bull.* **2004**, *49*, 1554–1569. [[CrossRef](#)]
55. Hu, B.; Li, J.; Cui, R.; Wei, H.; Zhao, J.; Li, G.; Fang, X.; Ding, X.; Zou, L.; Bai, F. Clay Mineralogy of the Riverine Sediments of Hainan Island, South China Sea: Implications for Weathering and Provenance. *J. Asian Earth Sci.* **2014**, *96*, 84–92. [[CrossRef](#)]
56. Zhong, Y.; Wilson, D.J.; Liu, J.; Wan, S.; Bao, R.; Liu, J.; Zhang, Y.; Wang, X.; Liu, Y.; Liu, X.; et al. Contrasting Sensitivity of Weathering Proxies to Quaternary Climate and Sea-Level Fluctuations on the Southern Slope of the South China Sea. *Geophys. Res. Lett.* **2021**, *48*, e2021GL096433. [[CrossRef](#)]
57. Gong, C.; Blum, M.D.; Wang, Y.; Lin, C.; Xu, Q. Can Climatic Signals Be Discerned in a Deep-Water Sink?: An Answer from the Pearl River Source-to-Sink Sediment-Routing System. *Bull. Geol. Soc. Am.* **2018**, *130*, 661–677. [[CrossRef](#)]
58. Wissink, G.K.; Hoke, G.D.; Garzante, C.N.; Liu-Zeng, J. Temporal and Spatial Patterns of Sediment Routing across the Southeast Margin of the Tibetan Plateau: Insights from Detrital Zircon. *Tectonics* **2016**, *35*, 2538–2563. [[CrossRef](#)]
59. Van Hoang, L.; Wu, F.Y.; Clift, P.D.; Wysocka, A.; Swierczewska, A. Evaluating the Evolution of the Red River System Based on in Situ U–Pb Dating and Hf Isotope Analysis of Zircons. *Geochem. Geophys. Geosyst.* **2009**, *10*. [[CrossRef](#)]
60. Clift, P.D.; Van Long, H.; Hinton, R.; Ellam, R.M.; Hannigan, R.; Tan, M.T.; Blusztajn, J.; Duc, N.A. Evolving East Asian River Systems Reconstructed by Trace Element and Pb and Nd Isotope Variations in Modern and Ancient Red River-Song Hong Sediments. *Geochem. Geophys. Geosyst.* **2008**, *9*. [[CrossRef](#)]
61. Li, C.; Lyu, C.; Chen, G.; Zhang, G.; Ma, M.; Yang, H.; Bi, G. Zircon U–Pb Ages and REE Composition Constraints on the Provenance of the Continental Slope-Parallel Submarine Fan, Western Qiongdongnan Basin, Northern Margin of the South China Sea. *Mar. Pet. Geol.* **2019**, *102*, 350–362. [[CrossRef](#)]
62. Wang, H.; Chen, S.; Gan, H.; Liao, J.; Sun, M. Accumulation Mechanism of Large Shallow Marine Turbidite Deposits: A Case Study of Gravity Flow Deposits of the Huangliu Formation in Yinggehai Basin. *Earth Sci. Front.* **2015**, *22*, 21–34. [[CrossRef](#)]
63. Li, C.; Lv, C.; Chen, G.; Zhang, G.; Ma, M.; Shen, H.; Zhao, Z.; Guo, S. Source and Sink Characteristics of the Continental Slope-Parallel Central Canyon in the Qiongdongnan Basin on the Northern Margin of the South China Sea. *J. Asian Earth Sci.* **2017**, *134*, 1–12. [[CrossRef](#)]

64. Rangin, C.; Klein, M.; Roques, D.; Le Pichon, X.; Le Van, T. The Red River Fault System in the Tonkin Gulf, Vietnam. *Tectonophysics* **1995**, *243*, 209–222. [[CrossRef](#)]
65. Clift, P.; Lee, G.H.; Anh Duc, N.; Barckhausen, U.; Van Long, H.; Zhen, S. Seismic Reflection Evidence for a Dangerous Grounds Miniplate: No Extrusion Origin for the South China Sea. *Tectonics* **2008**, *27*, 1–16. [[CrossRef](#)]
66. Liang, L. A Study of the Genesis of Hainan Island. *Geol. China* **2018**, *45*, 693–705. [[CrossRef](#)]
67. Liu, W.; Pei, J.; Yu, J.; Fan, C.; Zhang, X.; Shao, Y. Palaeogeomorphologic Control on Gravity Flow Deposit Sand Gas Reservoir Formation: A Case Study from the Miocene in Yinggehai Basin. *Mar. Geol. Quat. Geol.* **2017**, *37*, 197–203.
68. Zhang, J.; Fan, C.; Tan, J.; Chen, Y.; Huang, C.; Luo, W. Evolution Characteristics of Sedimentary System in Yinggehai Basin in Miocene and Its Exploration Significance. *Geol. Sci. Technol. Inf.* **2019**, *38*, 51–59.
69. Pohl, F.; Eggenhuisen, J.T.; Cartigny, M.J.B.; Tilston, M.C.; de Leeuw, J.; Hermidas, N. The Influence of a Slope Break on Turbidite Deposits: An Experimental Investigation. *Mar. Geol.* **2020**, *424*, 106160. [[CrossRef](#)]